AFRL-RV-PS-
TP-2012-0008

FIGURE TESTING AND CALIBRATION OF THE ISOON FABRY-PEROT ETALONS (POSTPRINT)

Brian Robinson, et al.

8 February 2012

Technical Paper

AIR FORCE RESEARCH LABORATORY
Space Vehicles Directorate
3550 Aberdeen Ave SE
AIR FORCE MATERIEL COMMAND
KIRTLAND AIR FORCE BASE, NM 87117-5776

REPORT DOCUMENTATION PAGE

Form Approved
OMB No. 0704-0188

1. REPORT DATE *(DD-MM-YYYY)*	2. REPORT TYPE	3. DATES COVERED *(From - To)*
08-02-2012	Technical Paper	1 Oct 2007 – 6 Oct 2011

4. TITLE AND SUBTITLE
Figure Testing and Calibration of the ISOON Fabry-Perot Etalons (Postprint)

5a. CONTRACT NUMBER

5b. GRANT NUMBER

5c. PROGRAM ELEMENT NUMBER
62601F

6. AUTHOR(S)
Brain Robinson, K.S. Balasubramaniam, Jerry Justice, Frank Pitts

5d. PROJECT NUMBER
1010

5e. TASK NUMBER
PPM00004579

5f. WORK UNIT NUMBER
EF004380

7. PERFORMING ORGANIZATION NAME(S) AND ADDRESS(ES)

Air Force Research Laboratory
Space Vehicles Directorate
3550 Aberdeen Ave SE
Kirtland AFB, NM 87117-5776

8. PERFORMING ORGANIZATION REPORT NUMBER

AFRL-RV-PS-TP-2012-0008

9. SPONSORING / MONITORING AGENCY NAME(S) AND ADDRESS(ES)

10. SPONSOR/MONITOR'S ACRONYM(S)
AFRL/RVBXS

11. SPONSOR/MONITOR'S REPORT NUMBER(S)

12. DISTRIBUTION / AVAILABILITY STATEMENT
Approved for public release; distribution is unlimited. (377ABW-2011-1072, 22 Jul 2011)

13. SUPPLEMENTARY NOTES
Solar Physics and Space Weather Instrumentation IV, Vol. 8148 81480A-1, DOI: 10.1117/12.892828, 6 Oct 2011.
Government Purpose Rights.

14. ABSTRACT
We present the methods and results for the figure testing and spectral calibration of the narrow- and wide-band etalons for the Improved Solar Observing Optical Network's dual-etalon tunable imaging filters. The ISOON system comprises a distributed network of ground-based patrol telescopes that gather full-disk data for the monitoring of solar activity and for the development of more reliable space weather models. The etalon figure testing consists mainly of testing the cavity flatness and coating uniformity of each etalon. For this testing a series of exposures is taken as the etalon is tuned through a stable spectral line and a full-aperture line profile correlation method is employed to map the variations in the effective cavity thickness. Calibration of the etalons includes absolute calibration of the cavity mean spacing change corresponding to a controller step and calibration of plate parallelism and spacing settings for each spectral region of interest. Developmental acceptance testing and calibration procedures were performed in a laboratory environment using a HeNe laser source. A calibration method that uses illumination in the telluric lines is also described. This latter method could be used to conduct calibration in the field without the use of an artificial light source.

15. SUBJECT TERMS
Fabry-Perot, Solar Telescope, Tunable Filters, Optical Testing, Space Weather, ISOON

16. SECURITY CLASSIFICATION OF:			17. LIMITATION OF ABSTRACT	18. NUMBER OF PAGES	19a. NAME OF RESPONSIBLE PERSON
a. REPORT	b. ABSTRACT	c. THIS PAGE	Unlimited	16	Donald Norquist
Unclassified	Unclassified	Unclassified			19b. TELEPHONE NUMBER *(include area code)*

Figure testing and calibration of the ISOON Fabry-Perot etalons

Brian Robinson[a], K.S. Balasubramaniam[b], Jerry Justice[c], Frank Pitts[c]

[a]University of Alabama in Huntsville, Ctr for Applied Optics, 301 Sparkman Dr., Huntsville, AL 35899
[b]Air Force Research Laboratory, USAF AFMC AFRL/RVBXS
[c]ARINC Engineering Services, LLC, 1925 Aerotech Drive, Suite 212
Colorado Springs, CO 80916-4219

ABSTRACT

We present the methods and results for the figure testing and spectral calibration of the narrow- and wide-band etalons for the Improved Solar Observing Optical Network's dual-etalon tunable imaging filters. The ISOON system comprises a distributed network of ground-based patrol telescopes that gather full-disk data for the monitoring of solar activity and for the development of more reliable space weather models. The etalon figure testing consists mainly of testing the cavity flatness and coating uniformity of each etalon. For this testing a series of exposures is taken as the etalon is tuned through a stable spectral line and a full-aperture line profile correlation method is employed to map the variations in the effective cavity thickness. Calibration of the etalons includes absolute calibration of the cavity mean spacing change corresponding to a controller step and calibration of plate parallelism and spacing settings for each spectral region of interest. Developmental acceptance testing and calibration procedures were performed in a laboratory environment using a HeNe laser source. A calibration method that uses illumination in the telluric lines is also described. This latter method could be used to conduct calibration in the field without the use of an artificial light source.

Keywords: Fabry-Perot, Solar Telescope, Tunable Filters, Optical Testing, Space Weather, ISOON

1 OVERVIEW OF THE ISOON SYSTEM

The main motivation for the ISOON system[1,2] is the need to provide synoptic visible band data without interruption in order to provide inputs for space weather prediction models and to provide a useful set of scientific data in the form of visible band spectroheliograms and vector magnetograms to the heliophysics community. Space weather, defined as the disturbances to the near-earth geomagnetic field and variability in high energy particle flux, can have adverse effects on military and civilian assets both in space and on the ground. Such adverse effects include damage to sensitive electronics aboard satellites, disruption of terrestrial power grids, and interference with ground-based radar installations. Full disk synoptic/patrol observations provide valuable data products for the development of ever more accurate space weather models used to predict and ameliorate the effects of solar-induced disturbances on important space- and ground-based infrastructure.

ISOON will be a remotely controlled network of solar imaging spectroscopic telescopes to continuously monitor the sun in several visible wave bands of interest. The data from the ISOON telescope are dark- and gain-corrected[2]. The resultant data is used to model the solar physical processes such as solar flares and coronal mass ejections at each wavelength and to predict their recurrence[3].

Schematics of the ISOON system[4] are shown in Figures 1-3. The critical elements providing spectral imaging for the ISOON system consists of a set of two Fabry-Perot Etalon filters in a standard imaging configuration[1,3]. ISOON uses a dual etalon system in a telecentric configuration that is similar to many solar and other optical telescope imaging systems that have preceded or followed it[5-9].

Solar Physics and Space Weather Instrumentation IV, edited by
Silvano Fineschi, Judy Fennelly, Proc. of SPIE Vol. 8148, 81480A
 · doi: 10.1117/12.892828

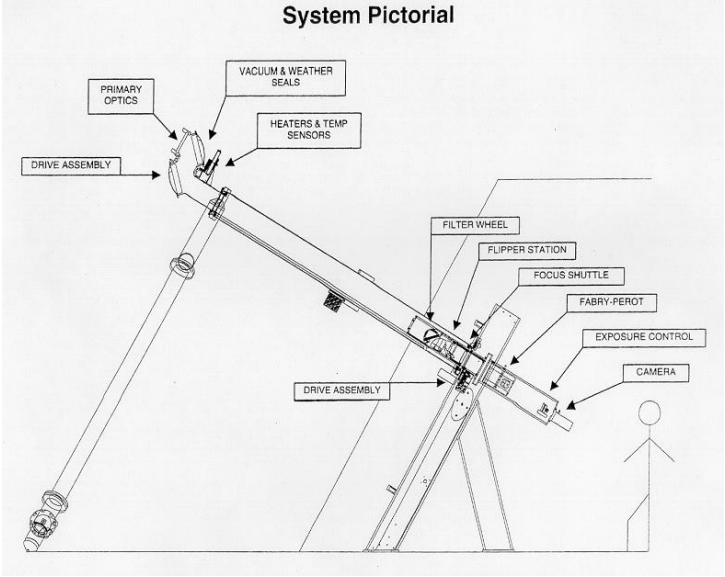

Fig. 1. Schematic of the ISOON telescope system.

Fig. 2. Photograph of the ISOON prototype facility at the NSO, Sacramento Peak campus.

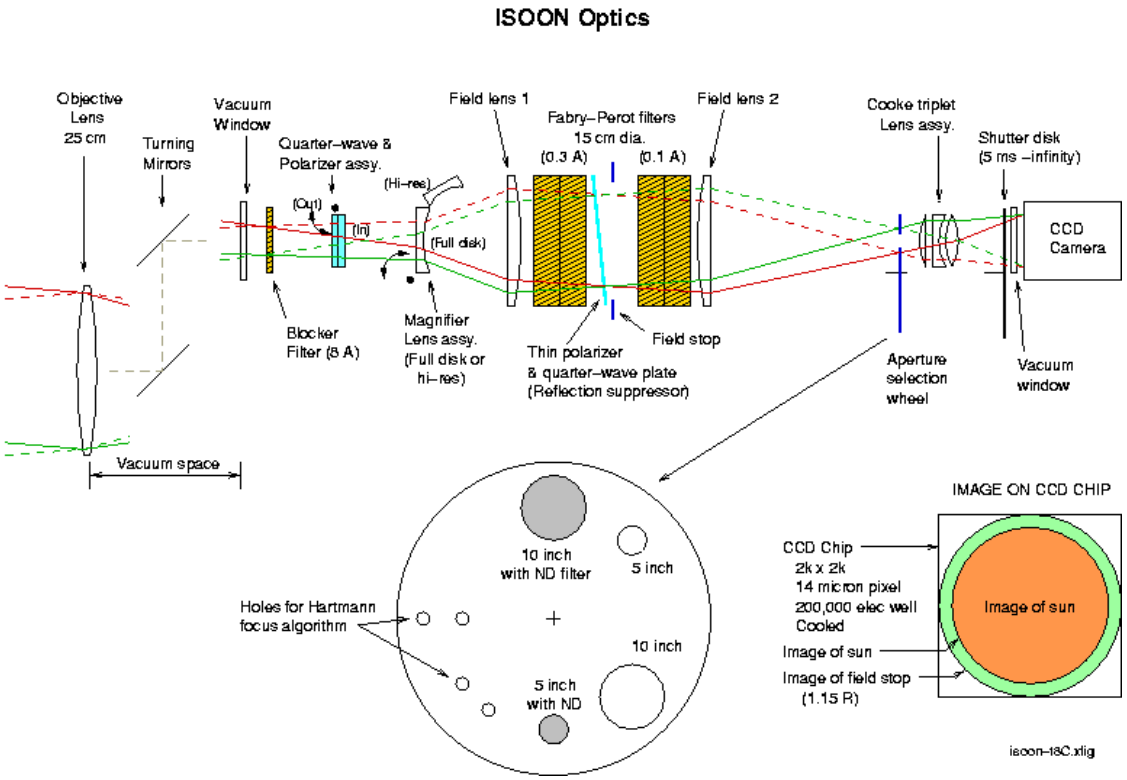

Fig. 3. Schematic of ISOON optical system.

Table1. ISOON Telescope Parameters

Parameter	Value
Aperture Diameter	250 mm
Field of View	32’ (full disk mode) / 9.3’ (high res mode)
Primary Focal Length	5000 mm
Bandpass	0.1 Å (0.1 – 0.25 Å depending on mode and F/#)
Detector	2048 x 2048 cooled CCD
Key Instrumentation	Dual F-P etalons, Polarization Analyzer
Pixel Size	14 microns: 1.1“ (full disk) / 0.32“ (high-res)
Photometric Accuracy	5 % over FOV, 12 bit intensity levels
Standard Cadence	1 H-α image per minute
Observed Wavelengths [Å]	6122 (CaI), 6302 (FeI), 6563 (Hα), 8542 (CaII), 10830 (HeI)
Nominal Spacing of Wide Etalon	3397286.476 Å
FWHM of Wide Etalon Peak	238 mÅ
Nominal Spacing of Narrow Etalon	12329607.814 Å
FWHM of Narrow Etalon Peak	65 mÅ

2 CALCULATION OF ETALON SPECIFICATIONS

When specifying the required cavity figure of each etalon in a dual etalon system, the tandem effects of figure errors must be taken into account. The spectral response uniformity requirement across the aperture dictates that the transmission peak of the dual etalon system should not deviate from the nominal wavelength by more than a quarter of the width of the nominal transmission profile at half maximum[7,8].

In order to determine the required surface figure for each etalon in the dual system, we begin with the tandem transmittance function for the pair, neglecting absorption:

$$T = T_1 T_2 = \frac{1}{1 + F_1 \sin^2\left(\frac{2\pi n d_1}{\lambda}\cos\theta\right)} \frac{1}{1 + F_2 \sin^2\left(\frac{2\pi n d_2}{\lambda}\cos\theta\right)} \ . \tag{1}$$

The coefficients of finesse are given by

$$F_1 = \frac{4R_1}{\left(1 - R_1\right)^2} \quad \text{and} \quad F_2 = \frac{4R_2}{\left(1 - R_2\right)^2} \ . \tag{2}$$

The spectral reflectances of the two etalons are assumed to be equal. Also we are considering airspaced etalons at normal incidence, so that the indices of refraction are equal to unity. The angle of incidence is considered to be zero, since we are only concerned with the location of the spectral resonance peaks here and not with the spread in the bandpass due to finite angles of incidence at the intermediate telecentric focus. The composite transmittance becomes

$$T = T_1 T_2 = \frac{1}{1 + F \sin^2\left(k d_1\right)} \frac{1}{1 + F \sin^2\left(k d_2\right)} \tag{3}$$

where

$$k = k_0 + \Delta k \quad ; \quad d_1 = d_{10} + \Delta d_1 \quad ; \text{and} \quad d_2 = d_{20} + \Delta d_2 \ . \tag{4}$$

Making these substitutions into the foregoing relationship, we obtain

$$T = \frac{1}{1 + F \sin^2\left[\left(k_0 + \Delta k\right)\left(d_{10} + \Delta d_1\right)\right]} \frac{1}{1 + F \sin^2\left[\left(k_0 + \Delta k\right)\left(d_{20} + \Delta d_2\right)\right]} \ . \tag{5}$$

Since Δk, Δd_1, and Δd_2 are very small compared with the nominal values, we can ignore the second order terms arising from the multiplications carried out within the square brackets:

$$T = \frac{1}{1 + F \sin^2\left(k_0 d_{10} + \Delta k d_{10} + k_0 \Delta d_1\right)} \frac{1}{1 + F \sin^2\left(k_0 d_{20} + \Delta k d_{20} + k_0 \Delta d_2\right)} \ . \tag{6}$$

The first terms in the sine arguments above represent the tuning of the etalons to a transmission peak. This together with the squaring of the sine functions implies that

$$T = \frac{1}{1 + F \sin^2\left(\Delta k d_{10} + k_0 \Delta d_1\right)} \frac{1}{1 + F \sin^2\left(\Delta k d_{20} + k_0 \Delta d_2\right)} \ . \tag{7}$$

Since we are looking at small deviations from the resonance condition, the sine functions above are approximately equal to their arguments, so that we can write

$$T = \frac{1}{1 + F\left(\Delta k d_{10} + k_0 \Delta d_1\right)^2} \frac{1}{1 + F\left(\Delta k d_{20} + k_0 \Delta d_2\right)^2} \quad . \tag{8}$$

Carrying out the multiplication on the bottom, we obtain

$$T = \frac{1}{1 + F k_0^2\left(\Delta d_1^2 + \Delta d_2^2\right) + \Delta k \cdot 2F k_0\left(\Delta d_1 d_{10} + \Delta d_2 d_{20}\right) + \Delta k^2 F\left(d_{10}^2 + d_{20}^2\right)} \quad . \tag{9}$$

The second term in the denominator represents an attenuation of the transmission peak due to the offset of the peaks of the individual etalon transmittance functions. Given the perturbations in the thickness of each cavity, this term is a constant. To estimate the peak of the composite response after the change of thickness in each etalon, the transmittance must be maximized by varying Δk. This implies minimizing the last two terms in the denominator. Taking the derivative of the two-term sum with respect to Δk and setting the result equal to zero, we obtain, after some algebra and considering only the absolute value of the shift of peak wavelength,

$$\Delta k = \left| \frac{k d_1}{d_1^2 + d_2^2} \Delta d_1 + \frac{k d_2}{d_1^2 + d_2^2} \Delta d_2 \right| . \tag{10}$$

To estimate the required peak-to-valley figure of each etalon, we assume the same cavity figure requirement for each etalon and examine the worst case in which the thickness of each etalon deviates by the maximum amount at the same place in the aperture. This implies the relation

$$\Delta\lambda = \lambda \frac{\left(d_1 + d_2\right)}{d_1^2 + d_2^2} \left|\Delta d\right| \quad . \tag{11}$$

The ISOON etalons have nominal spacings

$$d_1 = 1.233 \times 10^7 \text{ Å} \quad \text{and} \quad d_2 = 3.397 \times 10^6 \text{ Å}.$$

The full width at half maximum bandpass of the dual-etalon system in high-resolution, high-magnification mode, is required to be no more than 0.1 Å. To insure that the transmission peak at a wavelength of 6500 Å does not vary more than one quarter of this anywhere across the face of the etalon, the peak-to-valley departure of both etalons is calculated from the above equation to be less than +/- 40Å. This equates to a peak-to-valley figure of λ/80 at a test wavelength of 6328 Å.

After considering the perturbations to the thickness of each cavity to be independent, identically distributed, Gaussian random variables and applying the propagation of errors we obtain the following relationship between the standard deviation of the transmission peak as a function of the standard deviation of the cavity thicknesses:

$$\sigma_{\Delta\lambda} = \frac{\lambda}{\sqrt{d_1^2 + d_2^2}} \sigma_{\Delta d} \quad . \tag{12}$$

This makes sense given that the approximate relationship for a single etalon is

$$\frac{\Delta\lambda}{\lambda} = \frac{\Delta d}{d}.$$

For the case of two etalons with independent perturbations to the cavity thicknesses, the cavity thickness is replaced by the effective thickness $\sqrt{d_1^2 + d_2^2}$.

For the RMS deviation of the spectral peak to be half the size of the peak-to-valley deviation (i.e. one eighth of the full width at half maximum), we calculate the RMS deviation in the cavity thickness of each etalon from equation (12) to be +/- 25 Å. In other words this is an RMS cavity figure of λ/126 at a test wavelength of 6328 Å.

3 SPECTRAL CALIBRATION

For purposes of acceptance testing and calibration, each etalon must first have its average spacing and controller step size calibrated to a spectral reference. The spectral response of the etalons depends on spacing in a manner given by the factors in Equation (1). In order to have precise knowledge of spectral response of the etalon for a particular spacing command, the etalon spacing must be tied to an absolute spectral reference.

Terrestrial spectral lines can serve as this reference for *in situ* calibration and measurement. To calibrate the etalon spacing to a wavelength standard, the telluric line at 6301.991 Å (with a width of about 0.6 Å) can be employed. The ISOON system prefilter wheel includes a blocking filter at this wavelength. An added convenience in using this line is that the peak corresponding to an adjacent order of the narrow etalon falls in the continuum at a wavelength of 6303.6 Å allowing the transmission peak of the narrow etalon itself to be used to calibrate the spacing of the wide etalon as described below. Terrestrial spectral lines in the 6300 Å (6299.2 Å, 6302.0 Å) region are relatively stable [10] for purposes of direct optical calibration of etalons They are stable up to about 0.1 mÅ, whereas the spectral FWHM of the FP etalons in question are about 80-100mÅ , making them useful as standards.

The wide and narrow etalons must be adjusted in tandem to find the minimum of the telluric line. Since the FWHM of the narrow etalon peak is narrow compared to the width of the wide etalon peak, the peak of the transmission of the dual system is coincident with the peak of the narrow etalon, even if it is slightly misaligned from the peak of the wide etalon. If the dual system is tuned to the telluric line, so that the total illumination through the aperture is minimum, we can be assured that the peak of the narrow response is aligned in wavelength to the center of the absorption line. The dual scan is executed over about 25 controller steps and the position of the minimum is interpolated. The spacing sensed by the capacitance sensor on the narrow etalon now corresponds to the stable center of the telluric absorption line.

With the location of the narrow etalon peak determined, the adjacent narrow transmission order, which lies at 6303.6 Å, can be used to calibrate the spacing of the wide etalon. Since this peak lies in the continuum, it provides a clear maximum for this calibration. By scanning the wide etalon over several steps, the location of the transmission maximum can again be interpolated and the spacing of the wide etalon is now calibrated to the telluric line center.

With the passbands of the wide and narrow etalons pegged to the 6302 Å wavelength standard, the controller step size can be calibrated by scanning each etalon individually across the entire range of spacings while the other etalon is left static.

Note that the cavity figure, parallelism, and spacing can also be determined quite easily on the optics bench. In this case, each etalon can very easily be tested alone with a narrow emission line. This is a very convenient method for quickly determining acceptability of the etalons when they come from the manufacturer and for preliminary calibration of etalons, and it will be the method on which we concentrate here. The techniques above were developed so that all the calibration and cavity figure mapping could be done *in situ* without having to remove either of the etalons from the telescope. This would allow all these procedures to be accomplished remotely without intervention of a technician with wrenches and screwdrivers. As stated, the testing described here, however, was done in a laboratory environment using a HeNe laser at 6328 Å.

4 ETALON CAVITY FIGURE MEASUREMENT

Upon receipt of an etalon pair from the manufacturer, an acceptance test is performed to insure that the etalons meet specification, primarily in terms of cavity flatness. Due to the fact that the etalon are themselves very sensitive multiple beam interferometers, they can be easily used to test themselves. One simply has to project a stable, monochromatic, collimated beam through the etalon to examine the effective cavity figure. An accurate map of the cavity can be generated by stepping the etalon spacing through several (~100) increments in a programmed manner and processing the resulting data cube. A HeNe laser with spatial filter, collimating lens, and camera is sufficient (along with the etalon controller and software) to conduct this test.

To generate a cavity map from the acquired cube of data, the intensity profile of the scan is processed for each camera pixel. The simplest way to process the image data is to determine the location of each pixel's profile maximum. If a sufficient number of exposures is taken, the indices of all pixels' illumination maxima describe an acceptable map of the cavity flatness. The location of the maxima can also be interpolated for greater accuracy if needed. A more robust algorithm, which is more stable in the face of ambiguous maxima or anomalies in the data, is to use a correlation to map the cavity. In this scheme, a pixel near the center of the aperture is chosen as the reference. The profiles corresponding to all other pixels are correlated with this reference profile. The location, in terms of etalon spacing coordinate, of the resulting correlation maxima for all pixels within the etalon aperture are recorded and constitute a map of the etalon cavity.

A Fizeau interferometer with transmission reference removed can also be used in reflection to accomplish the same thing. In this case, the interferometer produces a collimated beam and the camera of the interferometer itself is used to record data. Furthermore, no tuning of the cavity is required if the interferometer is of the phase shifting type. We employed a non-phase-shifting Zygo Fizeau interferometer, with reference removed, to produce a collimated beam, since it was readily available and mapped the cavity via the scanning and correlating method described above.

Note that flatfielding is not a necessary step in either of the above mentioned figure testing methods. This is because we are looking for mutual shifts among the transmission profiles for each individual pixel, either via a search for the transmission maximum or via a search for a correlation maximum. In neither case are the results sensitive to the amplitude of the transmission profile (i.e. the flatfield) itself.

5 BENCHTOP TESTS OF A PAIR OF 150 MM CA ETALONS

The scanning method described above for measuring etalon cavity figure was applied to a pair of 150 mm diameter etalons of the same kind used in the current prototype ISOON facility and to be used in facilities to be deployed in the near future. The etalons were measured at facilities within the UAHuntsville Center for Applied Optics (see Figure 4) using a collimated HeNe beam and CCD camera. Controller step size, and therewith the scale of the figure errors, was determined by performing a cavity scan that contains three successive orders of transmission peaks (maxima of the average pixel irradiance). The positions of the peaks in units of controller steps were interpolated via parabolic fit, and the absolute size of a controller spacing step was determined as half the wavelength of the illuminating light divided by the average separation of peaks in terms of controller steps. Via this method, we determined that the absolute controller step size for the wide etalon to be 4.468 Å and for the narrow etalon to be 3.553 Å. This is in close agreement with the 4.662 Å and 3.547 Å measured for the same set of etalons about ten years ago at Sacramento Peak by Craig Gullixson. It is important to note that we did not use a stabilized laser to perform this development effort. Though the HeNe laser is inherently quite stable and provides a valid standard for measurement, a stabilized source would provide more accurate results.

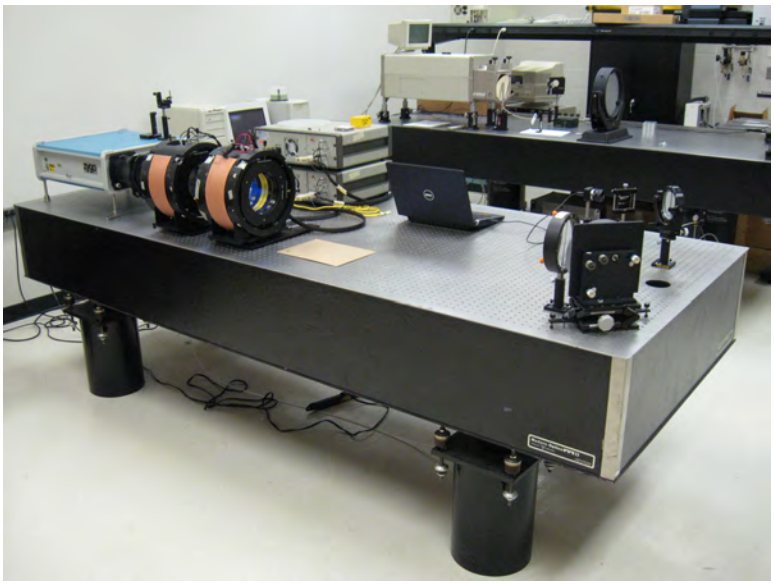

Fig. 4. Etalon test arrangement at UAHuntsville Center for Applied Optics

Figure 5 depicts the raw cavity figure of a pair of etalons. The first is an order sorting etalon with a spectral peak width of about 250 m Å, including the spread due to the finite ray cone angles within the telecentric image space in which it is located. The second is a spectrographic etalon with a narrow width of about 95 m Å. Figure 6 shows the same etalons with a low-pass filter applied in the form of a 45th order Zernike expansion. The low-pass filter was applied for three reasons. First we wanted to smooth over the faint fringes evident from the use of coherent illumination along with any aberrant data points that may skew the peak-to-valley reading. Second, the true cavity figure should have piston and tilt removed to accurately depict the figure at optimum parallelism and at best tuned cavity spacing. A third reason is that these truncated Zernike spectra are mathematically convenient and are employed in an analysis to be described below.

An important thing to note is that the Zernike tilt coefficients measured from the cavity scan are a direct quantification of the cavity parallelism. This information can be used to calibrate the x- and y-axis controller settings to achieve parallelism at this wavelength without the need for flatfielding. The as-tested x-tilt coefficient of the wide etalon was -28.3 Å (which corresponds to a maximum departure of half of this, or -14.2 Å, at the edge of the aperture) and the y-tilt coefficient was 8.5 Å (a 4.3 Å maximum departure). For the narrow etalon the coefficients were -0.9 Å and 4.8 Å with corresponding maximum departures of -0.5 Å and 2.4 Å, respectively. Although it was not completed as a part of this testing, the corresponding optimum settings for x and y parallelism would be almost trivial to determine, by measuring the response of the Zernike tilts to x and y controller axis settings.

These two etalons are an old set of prototypes that we used to try out our testing methods and develop control and data acquisition software (in Matlab). The salient feature of the data is the presence of rather severe figure errors near the edge of the etalon apertures. The peak-to-valley figure of the wide etalon is about 450 Å (λ/14 at 6328) and the RMS figure is about 87 Å (λ/72). For the narrow etalon, the measured P-V figure is 336 Å (λ/19) and the RMS figure was measured at 56 Å (λ/113). The results demonstrate that much of the aperture area has good figure, but the peak-to-valley departure is driven up by errors near the aperture edge. This is a typical error profile for large cavity Fabry-Perot etalons but is somewhat pronounced in these units. Given that the maximum acceptable P-V departure for an etalon is λ/80 (at 6328 Å), these two units are far out of spec.

6 SPECTRAL RESPONSE UNIFORMITY AND ANGULAR TUNING

Using Equation (10), the composite spectral response uniformity can be calculated for the pair of etalons. Figure 7 shows this uniformity in the form of peak wavelength shift in Å for the mutual orientation in which the etalons were tested. The peak-to-valley shift of the spectral peak across the etalon aperture in this configuration is 196 mÅ and the

RMS shift is 35 mÅ. The possibility of calculating this composite spectral performance raised the possibility of tuning the mutual angular (clocking) orientation of the two etalons to achieve optimum spectral response uniformity.

Using the Zernike decompositions calculated previously it is a simple matter to rotate the cavity figure map of one of the etalons while holding the other still. It is just a matter of performing the Zernike sum of one of the etalons (the spectrographic etalon in our case) in a rotated Zernike basis. Working in the Zernike representation also simplifies the process of insuring each set of cavity data has the same resolution for later processing. We performed the mutual rotation of the data sets, divided into 100 discrete steps from zero to 360°, and plotted the mean transmittance and RMS spectral shift within the aperture as a function of mutual clocking angle. These plots are shown in Figures 8 and 9 below. It is advantageous that the mean transmittance, ranging from about 46.2% to 49.6%, does not vary much as a function of mutual clocking angle of the etalons. This means we can vary the clocking angle to tune only the spectral response uniformity of the dual etalon system. The minimum RMS spectral error is seen to occur at a clocking angle of about 315°. The resulting spectral response uniformity (Figure 10) is significantly improved with a peak-to-valley shift of the spectral peak of 145 mÅ and an RMS shift of 25 mÅ. The mean transmittance in this configuration is around 47%, a negligible change.

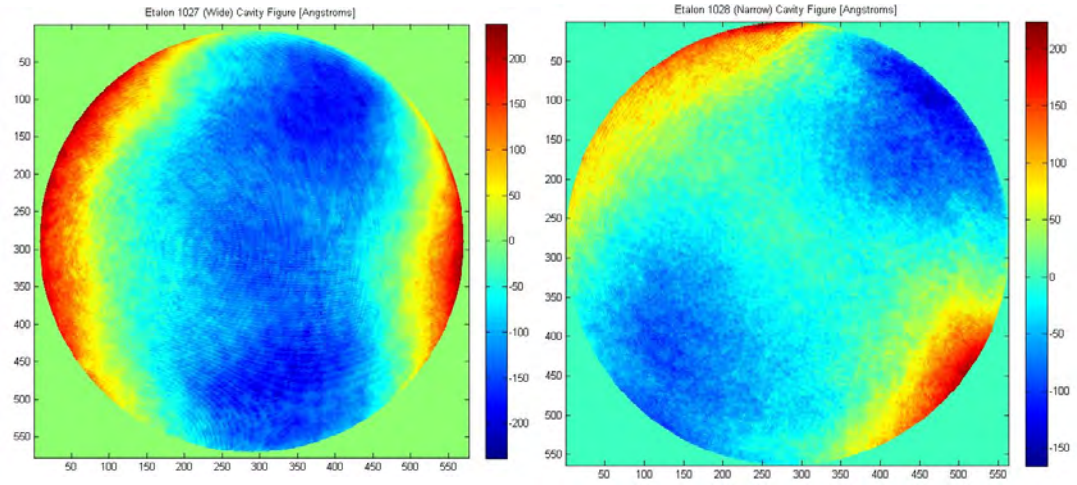

(a) (b)

Fig. 5. Raw cavity figure of (a) the spectrally wide, order-sorting etalon and (b) the narrow spectrographic etalon.

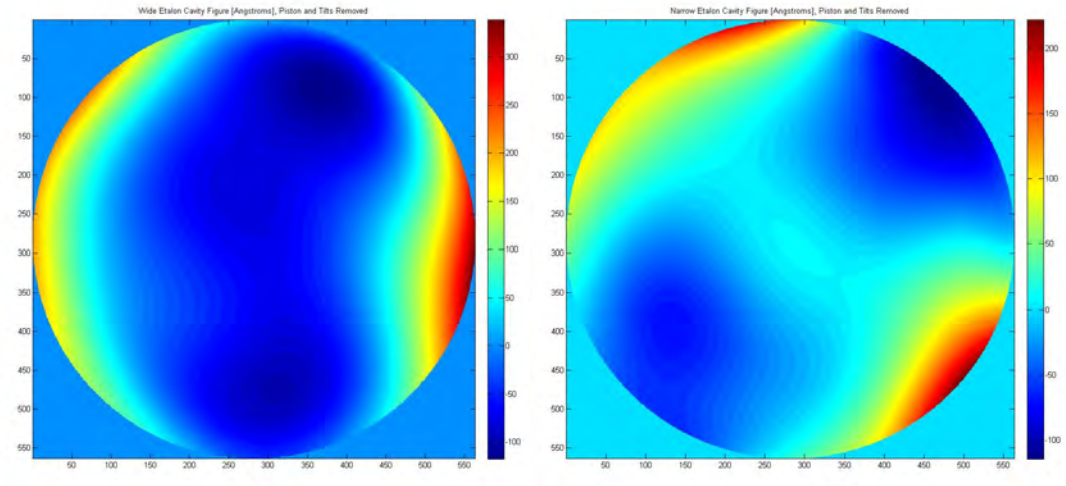

(a) (b)

Fig. 6. Filtered cavity figure of (a) wide etalon and (b) narrow etalon. Note that piston and tilt has been removed from the data.

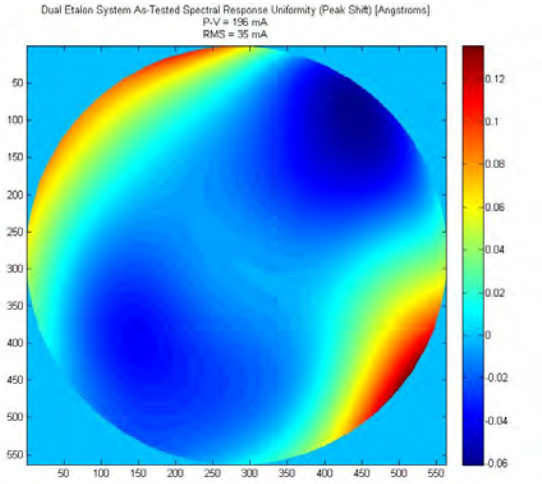

Fig. 7. Spectral response uniformity over the dual etalon system clear aperture in terms of shift of transmission peak, in Å.

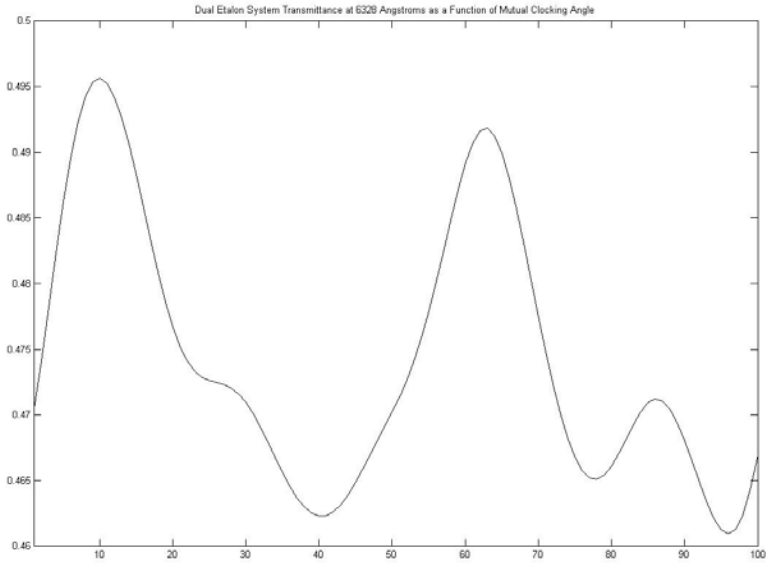

Fig. 8. Mean transmittance over the dual etalon system clear aperture as a function of mutual clocking angle of the two etalons. Note that there is not much variation.

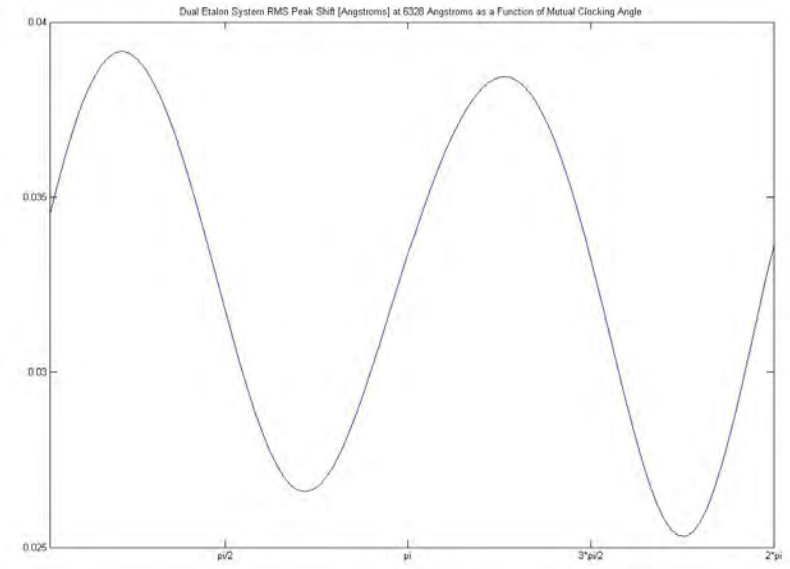

Fig. 9. RMS spectral response uniformity of the dual etalon system as a function of mutual clocking angle of the two etalons.

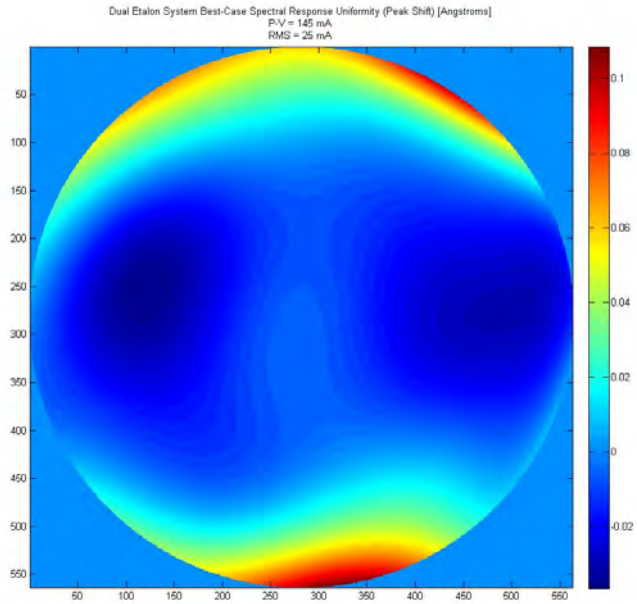

Fig. 10. Spectral response uniformity of the dual etalon system at optimum mutual clocking angle. The spectral performance is significantly improved while maintaining throughput.

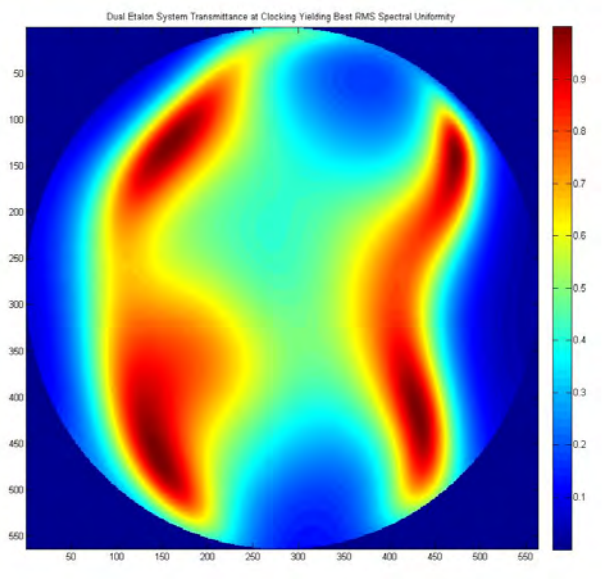

Fig. 11. Transmittance of the dual etalon system at clocking angle that yields optimum spectral performance. Note the dark areas within the clear aperture. This demonstrates the continued need for high-quality etalons to maintain good spectral performance and transmittance simultaneously.

7 FUTURE WORK

In this section we briefly propose a new method for measuring cavity figure and parallelism simultaneously, while the etalons are in the telescope, without need for prior flatfielding. This lack of dependence on flatfielding is necessary, since the flatfielding itself[2] takes into account the etalon transmittance (along with the effects of all other optics in the telescope), which can itself be affected by parallelism. The result of the cavity figure testing is a map of the cavity thickness, including tilt of the plates, which can be removed directly via a decomposition of the cavity figure into the Zernike polynomial basis.

To measure the cavity figure at each point in the aperture, we propose tuning the etalons in tandem to the center of the telluric line at 6302 Å. Then we would detune each etalon individually several controller steps in each direction to produce a discrete line profile for each pixel within the aperture. Given the nominal spacing of the etalons and the transmission profile of the telluric line, the resulting profiles can be expressed mathematically up to the free parameters describing the shift in spectral response of each etalon arising from cavity errors and the amplitude of each profile (which changes according to flatfield). These free parameters would be varied until the measured profiles match the theoretical profiles in the least-squares sense. The resulting shift parameters that are fit to the scan data would encode the cavity errors for the etalons. These cavity errors could be decomposed into the Zernike polynomial basis. In this way the cavity parallelism would directly appear, as above, as the two Zernike tilt coefficients. For accuracy this procedure can be repeated several times to provide a better estimate of the cavity figure as well as an estimate of the variance, due to errors and noise, in the regressed figure and parallelism.

8 SUMMARY AND CONCLUSIONS

We have summarized the operational system and science objectives of the ISOON solar telescope network and outlined the procedures for acceptance testing and characterization/calibration of the etalon systems. We have also presented the results of cavity figure measurement of two large prototype etalons conducted at the UAHuntsville Center for Applied Optics. The Matlab software and testbed we developed represent a very cost-effective and elegant arrangement for the acceptance testing and calibration of Fabry-Perot etalons on the optical benchtop. Future work should concentrate on refinement of these methods and, more importantly, on the development of a parallel program for testing and calibration that can be executed *in situ*, so that the cavity figure, parallelism, and spectral calibration can be monitored and updated

remotely, since one of the main requirements of the ISOON facilities' operation is that it can be done remotely, from a central location, though the facilities will be distributed at several locations across the planet.

9 REFERENCES

[1] Neidig, D. et al., "The USAF Improved Solar Observing Optical Network (ISOON) and its impact on solar synoptic data bases," in *ASP Conf. Ser. 140, Synoptic Solar Physics*, ed. Balasubramaniam, K.S., Harvey, J. and Rabin, D., p. 519 (1998).

[2] Dalrymple, N. E., Bianda, M. and Wiborg, P. H., "Fast flat fields from scanning extended sources," Publication of the Astronomical Society of the Pacific, vol. 115, pp. 628-34 (2003).

[3] Hernandez, G., [Fabry-Perot Interferometers], Cambridge University Press (1986).

[4] http://nsosp.nso.edu/isoon/

[5] Balasubramaniam, K.S. et al, "Sequential chromospheric brightenings beneath a transequatorial halo coronal mass ejection," The Astrophysical Journal, vol. 630, pp. 1160-67 (2005).

[6] Cavallini, F. et al., "Italian panoramic monochromator for the THEMIS telescope: the first results and instrument evaluation," Proc. SPIE 3355, p. 940-946, Optical Astronomical Instrumentation, Sandro D'Odorico; Ed. (1998)

[7] Balasubramaniam, K.S., "Imaging Spectroscopy of a Sunspot: Thermal and Velocity Structure," The Astrophysical Journal, vol. 575 no. 1, pp. 553-70 (2002).

[8] Robinson, B., Balasubramaniam, K.S., and Gary, G.A., "Advanced Technology Solar Telescope multiple Fabry-Pérot interferometer telecentric optical design," Optical Engineering,vol. 45 no. 2, 023001 (2006).

[9] Robinson, B., Gary, G.A. and Balasubramaniam, K.S.,"Evolution Strategies Optimization of the Multiple Fabry-Perót Imaging Interferometer for the Advanced Technology Solar Telescope," Optical Engineering, vol. 47, no. 10, 103002 (2008).

[10] Caccin, B. et al., "Terrestrial O2 lines used as wavelength references: experimental profiles and asymmetries vs. model computations," Astronomy and Astrophysics (ISSN 0004-6361), vol. 149, no. 2, Aug. 1985, p. 357-364. (1985).

ACKNOWLEDGMENTS

We would like to acknowledge Craig Gullixson of the National Solar Observatory for his invaluable technical contributions to the work described here, in the form of numerous face-to-face conversations, emails, and phone calls.

DISTRIBUTION LIST

DTIC/OCP
8725 John J. Kingman Rd, Suite 0944
Ft Belvoir, VA 22060-6218 1 cy

AFRL/RVIL
Kirtland AFB, NM 87117-5776 2 cys

Official Record Copy
AFRL/RVBXS/Donald Norquist 1 cy